



Synaptotagmin-7 deficiency induces mania-like behavioral abnormalities through attenuating GluN2B activity

Qiu-Wen Wang^{a,1}, Si-Yao Lu^{a,1}, Yao-Nan Liu^{a,1}, Yun Chen^a, Hui Wei^b, Wei Shen^a, Yan-Fen Chen^a, Chong-Lei Fu^a, Ying-Han Wang^a, Anbang Dai^a, Xuan Huang^c, Fred H. Gage^{d,2}, Qi Xu^{b,2}, and Jun Yao^{a,2}

^aState Key Laboratory of Membrane Biology, Tsinghua-Peking Center for Life Sciences, IDG/McGovern Institute for Brain Research, School of Life Sciences, Tsinghua University, 100084 Beijing, China; ^bState Key Laboratory of Medical Molecular Biology, Institute of Basic Medical Sciences Chinese Academy of Medical Sciences and Peking Union Medical College, Neuroscience Center, Chinese Academy of Medical Sciences, 100005 Beijing, China; ^cMedical Research Center, Beijing Chao-Yang Hospital, Capital Medical University, 100020 Beijing, China; and ^dLaboratory of Genetics, The Salk Institute for Biological Studies, La Jolla, CA 92037

Contributed by Fred H. Gage, October 2, 2020 (sent for review August 6, 2020; reviewed by Colleen A. McClung and Chun-Li Zhang)

Synaptotagmin-7 (Syt7) probably plays an important role in bipolar-like behavioral abnormalities in mice; however, the underlying mechanisms for this have remained elusive. Unlike antidepressants that cause mood overcorrection in bipolar depression, *N*-methyl-D-aspartate receptor (NMDAR)-targeted drugs show moderate clinical efficacy, for unexplained reasons. Here we identified Syt7 single nucleotide polymorphisms (SNPs) in patients with bipolar disorder and demonstrated that mice lacking Syt7 or expressing the SNPs showed GluN2B-NMDAR dysfunction, leading to antidepressant behavioral consequences and avoidance of overcorrection by NMDAR antagonists. In human induced pluripotent stem cell (iPSC)-derived and mouse hippocampal neurons, Syt7 and GluN2B-NMDARs were localized to the peripheral synaptic region, and Syt7 triggered multiple forms of glutamate release to efficiently activate the juxtaposed GluN2B-NMDARs. Thus, while Syt7 deficiency and SNPs induced GluN2B-NMDAR dysfunction in mice, patient iPSC-derived neurons showed Syt7 deficit-induced GluN2B-NMDAR hypoactivity that was rescued by Syt7 overexpression. Therefore, Syt7 deficits induced mania-like behaviors in mice by attenuating GluN2B activity, which enabled NMDAR antagonists to avoid mood overcorrection.

synaptotagmin 7 | mental disorder | bipolar disorder | mania | induced pluripotent stem cell

Despite past efforts to identify susceptible genes in patients, the pathogenesis of bipolar disorder (BD) has remained enigmatic, largely due to its complex multigenic origin. However, pedigree analysis has suggested a strong heritability of BD symptoms, indicating that the molecular and cellular deficits key for the mood abnormalities can be highly focused and stably inherited. Given that ~40% of BD patients show symptoms of insulin metabolic syndrome (1–3), it is possible that the behavioral and metabolic abnormalities in BD originate from an identical molecular mechanism functioning in the brain and pancreas. Guided by these clues, genes involved in both insulin metabolism and neuronal signaling have been investigated in the neurons derived from induced pluripotent stem cells (iPSCs) of BD patients and mice, leading to the identification of synaptotagmin-7 (Syt7) as a key factor in bipolar-like behavioral abnormalities (4). Significantly reduced Syt7 expression was observed in the blood and iPSC neurons of BD patients; moreover, Syt7 knockout (KO) mice showed circadian-based fluctuation of mania- and depression-like behavioral abnormalities. Syt7 has been suggested to be a high-affinity Ca²⁺ sensor for vesicle release. Via its two Ca²⁺-binding domains, C2A and C2B, Syt7 interacts with low-concentration Ca²⁺, SNAREs, and phospholipids to induce robust membrane fusion (5). In pancreatic β-cells, Syt7 is essential for the ignition of glucose-stimulated insulin secretion (6, 7). In the brain, Syt7 plays important roles in the action potential (AP)-triggered asynchronous neurotransmitter release, the fast synchronous form release during short-term synaptic plasticity, and

the slow phase of synaptic vesicle (SV) endocytosis (8–12). In addition, Syt7 can function with the redundancy of Syt1 to mediate the trafficking of the postsynaptic glutamate receptor α-amino-3-hydroxy-5-methyl-4-isoxazolepropionic acid receptor (AMPA) (13).

N-methyl-D-aspartate receptors (NMDARs), another major type of glutamate receptor, have long been known to be involved in neuropsychiatric disorders (14). For instance, ketamine, an NMDAR antagonist that has been recently approved for the clinical treatment of depressive disorders, likely exerts antidepressant effects through antagonizing the GluN2B subunit of NMDARs (15–18). Interestingly, while ketamine can often induce manic or psychotic symptoms in individuals without neuropsychiatric disorders (19), it has promising effects on patients suffering bipolar depression, because it rarely causes mood overcorrection issues (20–24). This efficacy is in sharp contrast to other major types of antidepressants, such as tricyclic antidepressants and selective serotonin reuptake inhibitors, which cause mood switching

Significance

Although synaptotagmin-7 (Syt7) has been found to play an important role in bipolar-like behavioral abnormalities in mice, the molecular mechanisms underlying the aberrant behaviors remain unknown. The reason for the promising efficacy of *N*-methyl-D-aspartate receptor (NMDAR) antagonists, such as ketamine, in the treatment of bipolar depression is also unclear. In the present study, we demonstrated that in human induced pluripotent stem cell-derived and mouse hippocampal neurons, Syt7 triggered glutamate release in the peripheral active zone, which efficiently activated juxtaposed postsynaptic GluN2B-NMDARs. As a result of the Syt7 deficits, GluN2B-NMDARs became hypoactive and consequently generated antidepressant effects, which induced mania-like behavioral abnormalities in the animals.

Author contributions: F.H.G. and J.Y. designed research; Q.-W.W., S.-Y.L., Y.-N.L., Y.C., H.W., W.S., Y.-F.C., C.-L.F., Y.-H.W., A.D., X.H., and Q.X. performed research; Q.-W.W., S.-Y.L., and J.Y. analyzed data; and J.Y. wrote the paper.

Reviewers: C.A.M., University of Pittsburgh School of Medicine; and C.-L.Z., The University of Texas Southwestern Medical Center.

The authors declare no competing interest.

Published under the [PNAS license](#).

¹Q.-W.W., S.-Y.L., and Y.-N.L. contributed equally to this work.

²To whom correspondence may be addressed. Email: gage@salk.edu, xuqi@pumc.edu.cn, or jyao@mail.tsinghua.edu.cn.

This article contains supporting information online at <https://www.pnas.org/lookup/suppl/doi:10.1073/pnas.2016416117/-DCSupplemental>.

First published November 23, 2020.

issues during the treatment of bipolar depression (25). Importantly, not only ketamine, but also other drugs targeting GluN2B-containing NMDARs or glutamatergic transmission, such as lamotrigine and riluzole, have no mood overcorrection effects (25, 26). Therefore, the glutamatergic system is likely involved in the pathophysiology of BD symptoms. However, how these drugs can avoid the induction of mood overcorrection in patients with bipolar depression has remained unclear.

In the present study, we found that in mouse hippocampal neurons, Syt7 activated GluN2B-NMDARs specifically in the peripheral synaptic region by triggering multiple forms of glutamate release. Thus, Syt7 deficiency induced GluN2B hypoactivity, which directly induced antidepressant behavioral consequences in the mice. As a result, GluN2B-NMDAR antagonists had a moderate effect on the Syt7 KO mice, which in turn generated antidepressant consequences and also avoided intense overcorrection responses. Furthermore, we identified

several SYT7 single nucleotide polymorphisms (SNPs) in BD patients and found that these mutations could induce GluN2B dysfunction and, consequently, mania-like behavioral abnormalities in the mice. Finally, we demonstrated that the human iPSC-derived hippocampal neurons showed identical Syt7/GluN2B dysfunctions that could be rescued by the overexpression of Syt7. Therefore, we concluded that the Syt7 deficit-induced GluN2B hypoactivity is likely a key mechanism behind the mania-like behaviors seen in the mice lacking functional Syt7.

Results

Dysfunction of GluN2B-Containing NMDARs Is Involved in the Mania-Like Behavioral Abnormalities of BD. NMDAR antagonists exert antidepressant effects, probably through inactivation of the GluN2B subunit (17, 27, 28). We tested the effects of NMDAR antagonists, including MK-801 (a nonselective NMDAR antagonist) and Ro25-6981 (a GluN2B-specific antagonist) on the

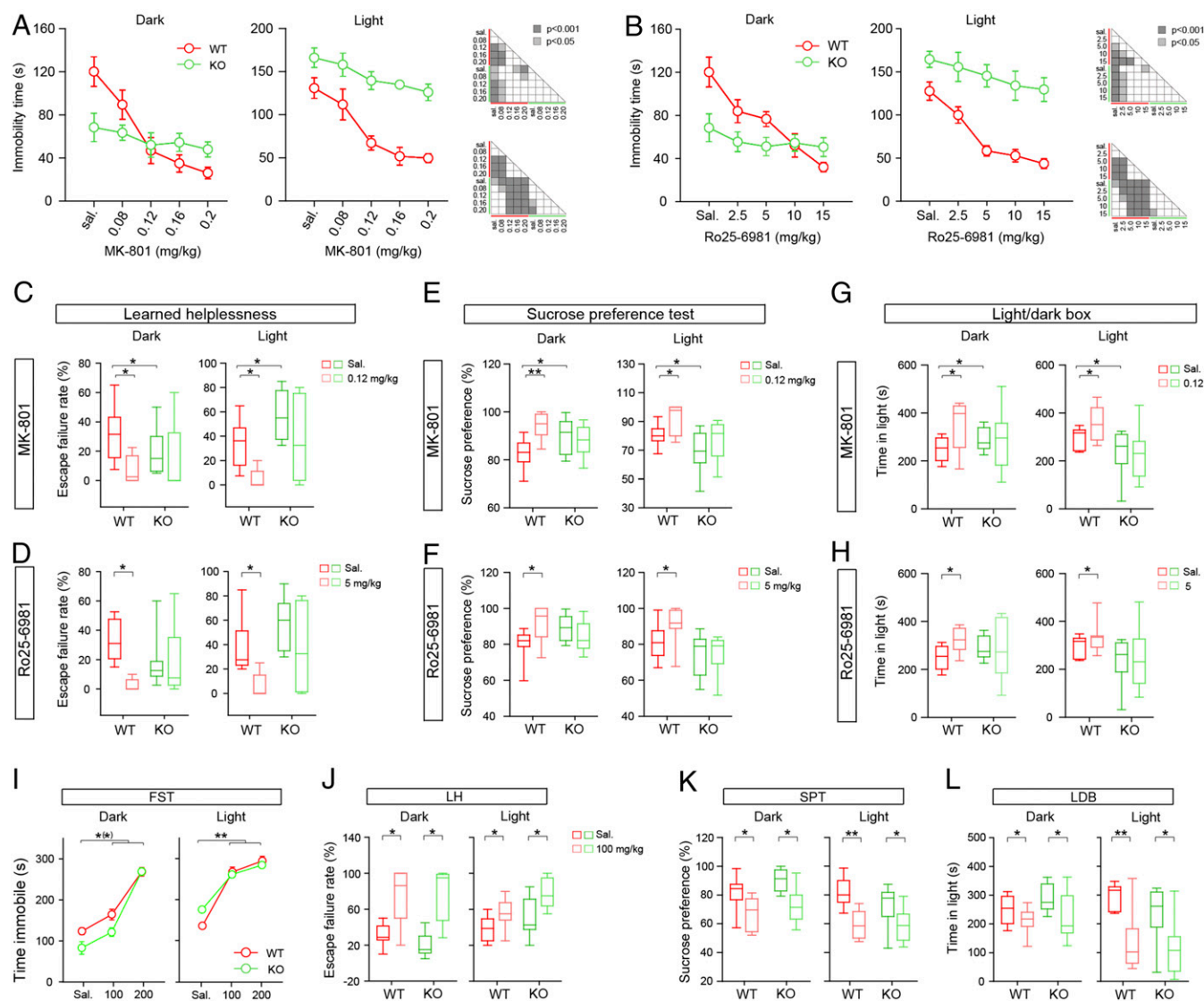


Fig. 1. NMDAR antagonists have moderate effects on the behavioral abnormalities of Syt7 KO mice. (A and B) Effects of MK-801 (A) and Ro25-6981 (Ro25) (B) on the FST immobility time in the dark (Left) and light (Right) phases. MK-801, 0.08 to 0.2 mg/kg; Ro25, 2.5 to 20 mg/kg. $n = 8$, ANOVA. (C and D) Effects of middle dose MK-801 (C; 0.12 mg/kg) and Ro25 (D; 5 mg/kg) on LH escape failure rate. WT, $n = 8$; KO, $n = 9$. (E and F) Sucrose preference ratio of mice treated with middle dose MK-801 (E) and Ro25 (F). $n = 10$. (G and H) Effects of middle dose MK-801 (G) and Ro25 (H) on LDB time in light. $n = 11$. (I) Effects of VPA (100 to 200 mg/kg) on FST immobility. $n = 8$, ANOVA. (J) Effects of low-dose VPA (100 mg/kg) on LH escape failure rate. WT, $n = 8$; KO, $n = 9$. (K and L) Effects of low-dose VPA on sucrose preference ratio (K) and LDB time in light (L). $n = 11$. * $P < 0.05$; ** $P < 0.01$, Student's t test. Error bars represent SEM.

behavioral abnormalities of the Syt7 KO mice using the forced swim test (FST), learned helplessness (LH) test, sucrose preference test (SPT), and light/dark box (LDB) test. Consistent with our previous report (4), compared with wild-type (WT) mice, the Syt7 KO mice had a shorter immobility time, a lower escape failure rate, a higher sucrose preference ratio, and a longer time in light in the dark phase (Zeitgeber time [ZT], 12 to 24), whereas they showed opposite results in the light phase (ZT 0 to 12) (Fig. 1A–G).

Through intraperitoneal injection, we tested the effects of a concentration gradient of MK801/Ro25-6981 on the FST. In the WT mice, starting from the middle concentration, the two drugs could induce drastic reductions in immobility time in both the dark and light phases (Fig. 1A and B). However, in the Syt7 KO mice, only the highest-concentration drug treatments restored the light phase immobility time to a normal level, and all drug treatments failed to show any significant effects in the dark phase. We then carried out LH and SPT experiments using middle doses of the drugs. In both phases, MK-801 (0.12 mg/kg) and Ro25-6981 (5 mg/kg) significantly reduced the LH escape failure rate and increased the sucrose preference ratio and LDB time in light in the WT mice; however, in the Syt7 KO mice, the drug treatments induced only slight changes (Fig. 1C–H). Thus, not only MK-801, but also the GluN2B-specific antagonist Ro25-6981 showed moderate effects on the behavioral abnormalities of the Syt7 KO mice. To further verify this observation, we tested the efficacy of valproic acid (VPA), a mood stabilizer, and found that both high and low doses of VPA could significantly affect the Syt7 KO mice (Fig. 1I–L), which verified the avoidance of the intense effects of NMDAR antagonists on the Syt7 KO mice. As MK-801 and Ro25-6981 had remarkable antidepressant effects on the WT mice, it is likely that the Syt7 KO mice had dysfunction of GluN2B-NMDARs, and that the derived antidepressant effects were crucial for the induction of the mania-like behavioral abnormalities in these mice.

Syt7 Triggers Glutamate Release in the Peripheral Active Zone to Activate GluN2B. To test how dysfunction of GluN2B-NMDARs is induced by Syt7 deficiency, we first used the superresolution stochastic optical reconstruction microscopy (STORM) technique to investigate the synaptic localization of Syt7 and GluN2B in hippocampal CA1 slices of mice. Antibodies specific for vGLUT1 and PSD95 were used to delineate the presynaptic boutons and postsynaptic density (PSD), respectively (Fig. 2A and B). The neurotransmission active site was determined with direct opposition of vGLUT1 and PSD95 within a detected range of 30 nm, which corresponds to the width of the synaptic cleft (29). In the WT neurons, the t-SNARE protein SNAP-25 was detected in the central active zone (AZ) in the majority of investigated synapses, whereas in most cases, Syt7 was ~100 nm (range, 60 to 170 nm) away from this region (Fig. 2C). As the length of the synaptic site (AZ/PSD) is usually 250 to 300 nm, this result indicates that Syt7 was largely located in the peripheral AZ.

We then analyzed the localization of GluN2B in comparison to GluN2A. In the WT mice, GluN2A penetrated deeply into the PSD, whereas GluN2B was mostly ~100 nm away from the central PSD (Fig. 2D and E), indicating that GluN2B was largely located in the peripheral and extrasynaptic areas. Moreover, GluN2B showed an identical distribution pattern in the WT and KO slices (Fig. 2E), indicating that the Syt7 deficiency would not affect the distribution of GluN2B. In addition, the GluN2B/PSD95 ratio was significantly increased in the Syt7 KO neurons (Fig. 2F and G), indicating enhanced expression of GluN2B. Immunoblot and quantitative reverse-transcription PCR (qRT-PCR) analyses confirmed the increased expression of GluN2B and other NMDAR subunits in the KO neurons, resembling that in WT neurons treated with Ro25-6981 (Fig. 2H and SI Appendix, Fig. S1). In the Ro25-6981-treated WT neurons, the increased GluN2B expression was likely caused by a

homeostatic adjustment (30), analogous to the “synaptic scaling” in which the blockade of AMPARs is seen to always lead to increased AMPAR expression (31). Thus, we hypothesized that the enhanced GluN2B expression in the Syt7 KO mice might also originate from insufficient activity of GluN2B.

We then carried out whole-cell patch clamp recordings in acutely dissected hippocampal slices to investigate the GluN2B activity in Syt7 KO mice. Consistent with previous studies (9–11), the Syt7 KO neurons did not show any obvious changes in single AP-evoked AMPAR-mediated excitatory postsynaptic currents (AMPA-EPSCs) but did show a more rapid depression in the amplitude of EPSCs evoked by a short train stimulation (20 Hz, 1 s) compared with the WT mice (SI Appendix, Fig. S2). Consistent with the enhanced expression of NMDAR subunits, the single AP-evoked NMDAR-EPSCs showed a significantly larger amplitude in the Syt7 KO neurons compared with the WT neurons (Fig. 2I). We applied Ro25-6981 to the recording system and found that the NMDAR-EPSC amplitude was only slightly reduced in both the WT and the Syt7 KO neurons (Fig. 2I), indicating that the GluN2B-NMDARs were not a major component of total NMDARs activated by a single AP. We then investigated the train stimulation-evoked NMDAR-EPSCs and found that the WT and Syt7 KO neurons showed similar cumulative charge transfer (Fig. 2J–L), which was different from the attenuated train-evoked AMPAR-EPSCs and probably resulted from the enhanced NMDAR expression in the Syt7 KO neurons. Although Ro25-6981 did not induce any obvious changes in either group, we observed that after the drug treatment, the total charge transfer of the Syt7 KO neurons was greater than that in the WT (Fig. 2L). Thus, the GluN2B-NMDARs could be activated to some extent by train AP firing in the WT hippocampal neurons, whereas in the Syt7 KO neurons, the GluN2B-NMDARs showed hypoactivity during short-term synaptic plasticity, in which Syt7 plays an important role.

Syt7 is probably a Ca^{2+} sensor for asynchronous release, which accounts for only ~20% of the total release (9, 32). To investigate whether GluN2B was activated by asynchronous release, we analyzed the train-stimulated AMPAR-EPSCs in the context of 0.2 mM $[\text{Ca}^{2+}]_i$, which mimicked the residual Ca^{2+} influx (Fig. 2M). Compared with the WT slices, the Syt7 KO slices showed obvious reductions in the amplitude of the first EPSCs and the total charge transfer of the train AMPAR-EPSCs (Fig. 2N). We then analyzed the train-evoked NMDAR-EPSCs and found that the WT and Syt7 KO slices showed similar levels of total charge transfer and delayed charge transfer (Fig. 2O and P) (12). Moreover, the Ro25-6981 treatment significantly reduced the total and delayed charge transfer in the WT mice but failed to obviously affect the Syt7 KO mice. Thus, GluN2B-NMDARs were activated by residual Ca^{2+} -triggered glutamate release in the WT mice, but such activation was largely diminished in the Syt7 KO neurons.

Taken together, our findings demonstrate that both Syt7 and GluN2B-NMDARs were localized to the peripheral synaptic region, and that GluN2B-NMDARs could be efficiently activated by Syt7-triggered glutamate release.

Human SYT7 SNPs Induce GluN2B Dysfunction and Mania-Like Behaviors in Mice. To determine whether the SYT7 gene itself is associated with the development of BD in humans, we performed Sanger sequencing analysis in the SYT7 coding regions of 1,456 BD patients and 1,202 controls. A total of five SNPs, including four missense mutations and one synonymous mutation, were identified in six BD patients, but no Syt7 mutation was found in any of the healthy control subjects (SI Appendix, Table S1). All mutations resided on exon 6 of the human SYT7 gene, which encodes the juxtamembrane linker region of the protein. The combined χ^2 test showed a significant correlation with BD ($\chi^2 = 4.965$, $P = 0.0259$; OR, 10.78; 95% CI, 0.6061 to 191.6). A harmfulness evaluation of the four missense mutations was performed on

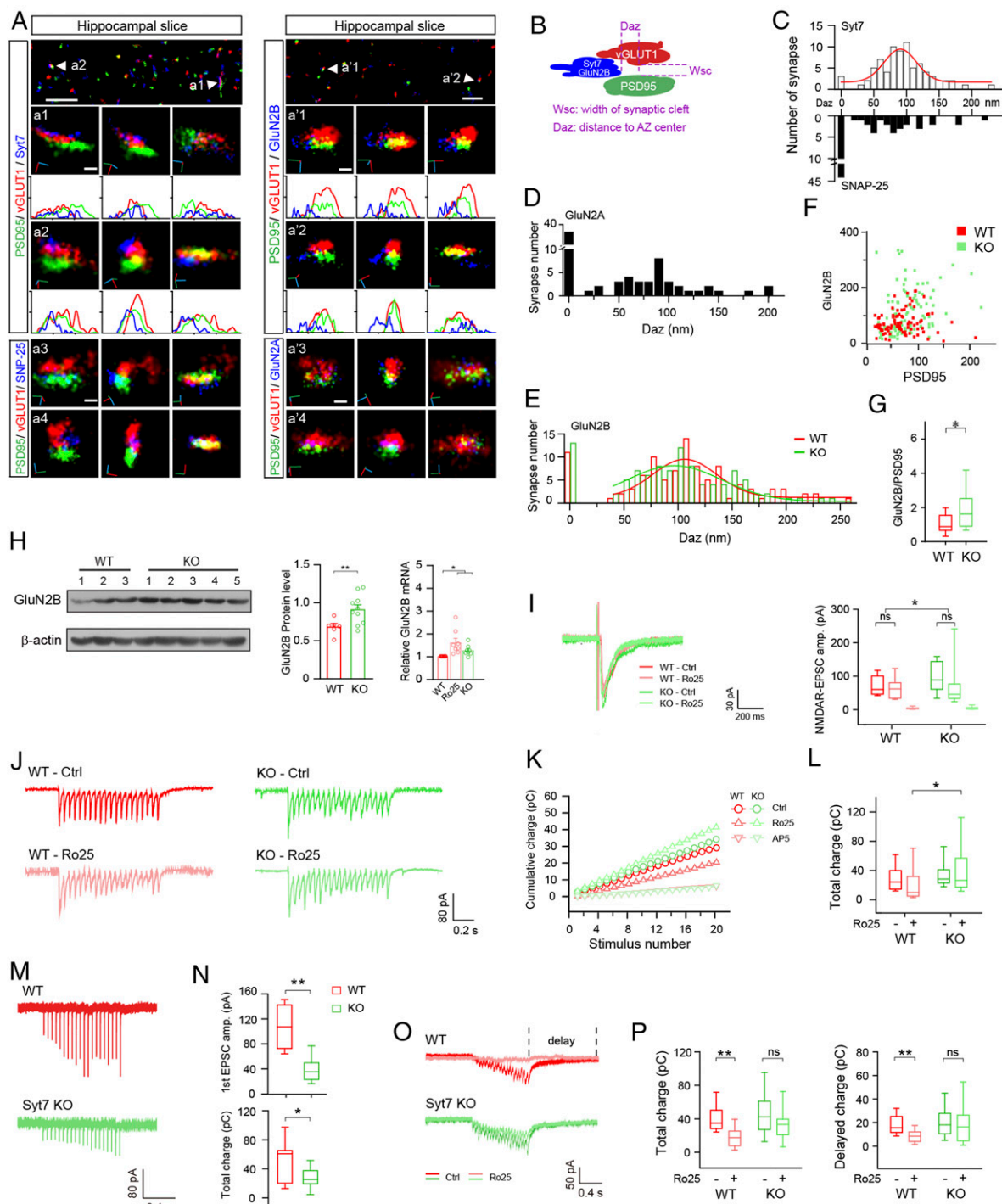


Fig. 2. Syt7 triggers glutamate release in peripheral AZ to activate GluN2B-NMDARs. (A) Sample STORM images of hippocampal slices showing localization of Syt7 (Left) and GluN2B (Right) in the synapses. (a1–a4) From Left to Right, the face view, side view, and view along the transsynaptic axis of sample synapses showing the localization of Syt7 (a1 and a2) and SNAP-25 (a3 and a4). (a'1–a'4) Localization of GluN2B (a'1 and a'2) and GluN2A (a'3 and a'4). Curves indicate the fluorescence intensity projected onto the x-axis. (Scale bars: 2 μm in the Top images, 100 nm in the Bottom images.) (B) Schematic of the analytic model for quantifying the distance of tested proteins to the center of the AZ. (C) Histograms showing the shortest distance of the Syt7/SNAP-25 signal to the AZ center. Syt7, $n = 76$; SNAP-25, $n = 71$. The red curve represents the fitted Gaussian curve. (D and E) Shortest distance of the GluN2A (D; $n = 75$) and GluN2B (E; $n = 73$) signals to the PSD center. (F) Number of GluN2B localization points vs. number of PSD95 localization points for each synapse. (G) Quantification of GluN2B/PSD95 ratio. (H) Immunoblot (Left) and quantification (Middle) of GluN2B in hippocampal tissues and qRT-PCR data (Right) of GluN2A/2B in cultured hippocampal neurons. (Left) WT, $n = 6$; KO, $n = 10$. (Middle and Right) $n = 9$ for both groups. (I) Sample traces (Left) and mean amplitude (Right) of 2 mM $[\text{Ca}^{2+}]$ evoked NMDAR-EPSCs in hippocampal slices. WT, $n = 20/17/9$; KO, $n = 29/17/13$. (J–L) Sample traces (J), cumulative charge transfer (K), and total charge (L) of 2 mM $[\text{Ca}^{2+}]$ evoked train NMDAR-EPSCs in hippocampal slices. WT, $n = 20/17$; KO, $n = 38/29$. (M) Sample traces of train evoked AMPAR-EPSCs in slices triggered by 0.2 mM Ca^{2+} . (N) Amplitude of the first EPSCs (Upper) and total charge of the train EPSCs (Lower). WT, $n = 8$; Syt7 KO, $n = 9$. (O) Sample traces of train NMDAR-EPSCs in slices triggered by 0.2 mM Ca^{2+} . (P) Total charge transfer (Left) and decay time constant (Right) of NMDAR-EPSCs. $n = 14$. * $P < 0.05$; ** $P < 0.001$, Student's t test. Error bars represent SEM.

PolyPhen-2 (genetics.bwh.harvard.edu/pph2/) based on the structure and functional predictions. Three of these mutations showed damage potential on the Syt7 protein structure: L227M, Q247H, and L314M.

We then carried out the behavioral examinations using human L227M and Q247H mutations as examples. In the mice, of the four isoforms of *SYT7*, two (γ and 4) had the exon containing these mutation sites. Thus, we compared the effects of isoform 4 of mouse Syt7 (Syt7^{IF4}) and its mutant carrying mutations corresponding to human L227M/Q247H (Syt7^{IF4mut}) (Fig. 3A and B). We suppressed Syt7 expression in the hippocampal dentate gyrus (DG) through local infusion of lentivirus encoding the Syt7-specific CRISPRi and simultaneously reintroduced Syt7^{IF4} or Syt7^{IF4mut}. The qRT-PCR analysis revealed that Syt7^{IF4} and Syt7^{IF4mut} were well expressed in the Syt7 knockdown (KD) mice (Fig. 3C). Behavioral analysis revealed that in the dark phase, compared with the WT scrambled controls, the Syt7 KD mice showed a significant reduction in the FST immobility time and obvious increases in the sucrose preference ratio and LDB time in light; moreover, the KD mice expressing Syt7^{IF4} showed an obvious alleviation of the behavioral abnormalities, whereas the KD mice expressing Syt7^{IF4mut} still showed behavioral abnormalities

similar to those in the KD mice (Fig. 3D–F). Therefore, human Syt7 L227M and Q247H mutations could lead to antidepressant behavioral consequences in the mice.

We next investigated the activity of GluN2B-NMDARs in neurons expressing Syt7^{IF4mut}. The qRT-PCR analysis revealed that the enhanced GluN2B expression in the Syt7 KO neurons was rescued by Syt7^{IF4}, but not by Syt7^{IF4mut}. Moreover, the Ro25-6981 treatment enhanced the expression of GluN2B in Syt7^{IF4}-expressing KO neurons, whereas the Syt7^{IF4mut}-expressing neurons were unaffected (Fig. 3G). We carried out a patch clamp recording analysis to investigate the train stimulation-evoked NMDAR-EPSCs in 0.2 mM [Ca²⁺] (Fig. 3H). The Ro25-6981 treatment induced significant reductions in EPSC charge transfer and decay time in the WT scrambled controls but failed to significantly affect the Syt7 KD neurons; moreover, expression of Syt7^{IF4} in the KD neurons rescued the resistance to the drug application, whereas the introduction of Syt7^{IF4mut} did not produce obvious changes (Fig. 3I and J). Thus, the Syt7^{IF4mut} mutant could not function to activate GluN2B-NMDARs. Taken together, our data indicate that the *SYT7* gene is associated with the susceptibility to BD in humans, and that the Syt7 SNPs

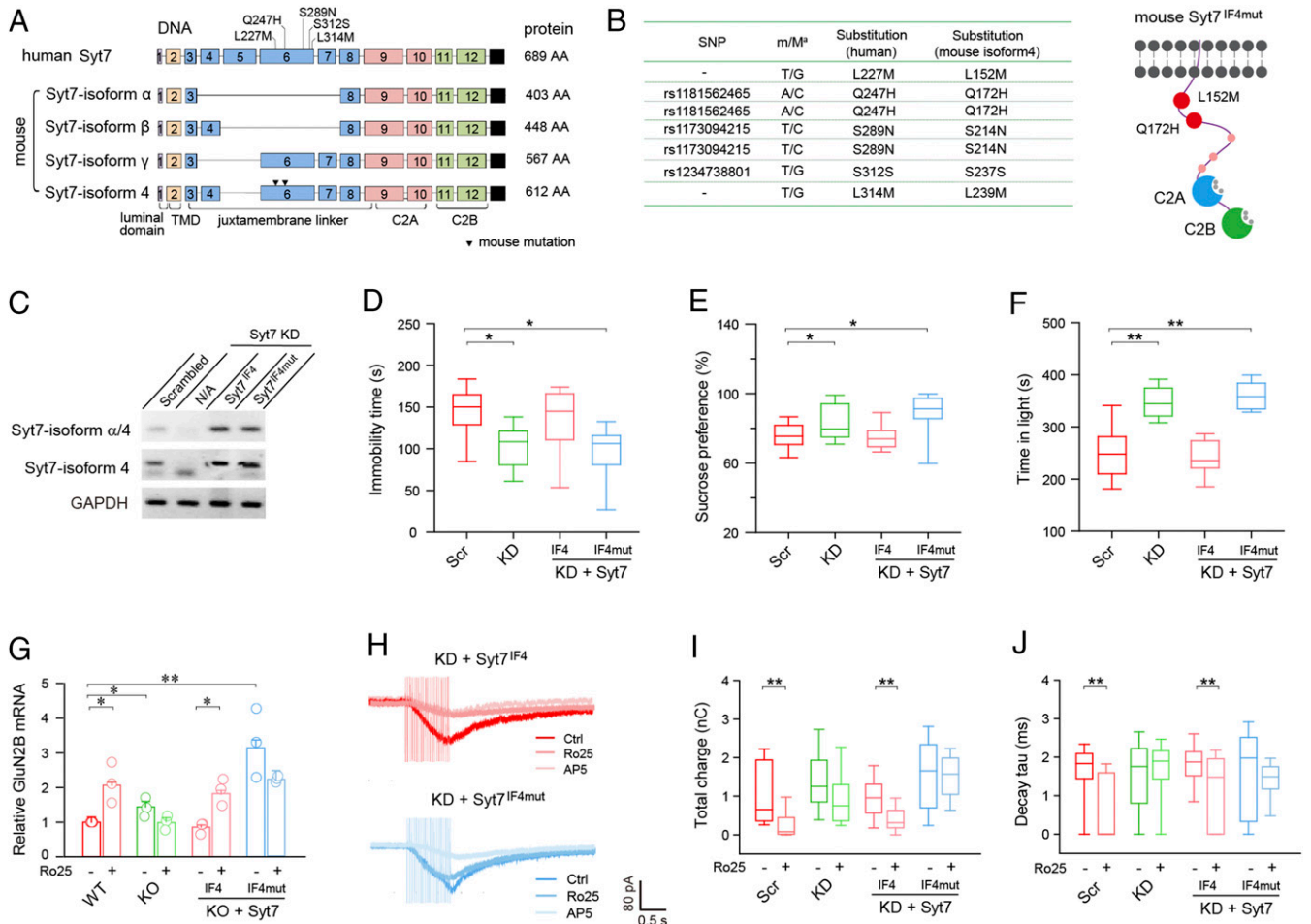


Fig. 3. Human Syt7 variants induce mania-like behaviors and GluN2B hypoactivity in mice. (A) Diagram showing mutations identified in exon 6 of the human Syt7 gene. (B) Table (Left) and schematic (Right) showing mouse Syt7 isoform 4 carrying two sample mutations (L152M/Q172H) in the juxtamembrane linker domain. (C) RT-PCR analysis showing CRISPRi-based Syt7 KD and reintroduction of Syt7^{IF4} or Syt7^{IF4mut}. (D–F) FST immobility time (D), sucrose preference ratio (E), and LDB time in light (F) of mice with Syt7^{IF4} or Syt7^{IF4mut} expressed in the hippocampus. $n = 15$. (G) qRT-PCR analysis of GluN2B in Syt7 KO neurons expressing Syt7^{IF4} or Syt7^{IF4mut}. $n = 3$. (H) Sample traces of 0.2 mM Ca²⁺-triggered train NMDAR-EPSCs in Syt7 KD neurons expressing Syt7^{IF4} or Syt7^{IF4mut}. (I and J) Total charge transfer (I) and decay time constant (J) of NMDAR-EPSCs. Scr, scrambled sgRNA. $n = 19$ for Ctrl and $n = 22$ for Ro25; Syt7 KD, $n = 17/14$; Syt7^{IF4}, $n = 27/19$; Syt7^{IF4mut}, $n = 12/16$. * $P < 0.05$; ** $P < 0.001$, Student's t test. Error bars represent SEM.

identified in BD patients could generate antidepressant effects in the mice through inducing GluN2B dysfunction.

Monitoring Syt7-Triggered Glutamate Release in the Peripheral AZ. To further our understanding of the glutamate release triggered by Syt7 or its SNPs in the peripheral AZ, we carried out a structured illuminating microscopy (SIM) analysis with pHluorin-tagged synaptophysin (sypHy) as a fluorescence reporter to directly monitor the SV exocytosis in the AZ of Syt7-defective neurons (Fig. 4*A* and *B*). The sypHy reporter is quenched by low pH in the SV lumen and dequenched by SV exocytosis, and changes in the sypHy signal represent bona fide presynaptic SV cycling events (33). The spatial resolution of the SIM system is ~100 nm, which is able to indicate where SV exocytosis occurs. At this resolution, the frame rate is ~0.4 Hz. To obtain sufficient data points for analysis, we elongated the protocol of the 20-Hz stimulation to a 10-s duration. As Syt7 showed strong interaction with residual Ca^{2+} to trigger SV release, we used 0.2 mM $[\text{Ca}^{2+}]$ to maximize the Syt7-specific release. Because Sr^{2+} is able to promote asynchronous release and Syt7 is a strong Sr^{2+} sensor (5, 12, 34), we used 0.2 mM $[\text{Sr}^{2+}]$ as a control means to acquire the maximal segregation of Syt7-triggered and non-Syt7-triggered SV release events. Meanwhile, we used 4 mM $[\text{Ca}^{2+}]$ as another control to characterize the exocytosis under high $[\text{Ca}^{2+}]$.

The imaging analysis revealed that in the WT neurons, the total amount and kinetics of exocytosis triggered by 0.2 mM Sr^{2+} were similar to those caused by 4 mM Ca^{2+} but greater than those caused by 0.2 mM Ca^{2+} . In contrast, in the Syt7 KO neurons, 0.2 mM Sr^{2+} triggered significantly less SV release compared with 0.2 mM Ca^{2+} , and the latter elicited much weaker exocytosis compared with 4 mM Ca^{2+} (Fig. 4*C* and *D*). Thus, Syt7 contributed significantly to the SV release elicited by residual levels of $[\text{Ca}^{2+}]$. Importantly, the phenotype of the Syt7 KO neurons was restored by reintroduction of Syt7^{FL} but not by Syt7^{IF4mut}, indicating that the Syt7 SNPs could not effectively elicit SV release.

To evaluate the location of the Syt7-triggered release, we next analyzed the changes in the full width of half maximal (FWHM) with the Gaussian distribution of the SypHy signals (Fig. 4*E* and *F*), which is quantified along the direction of the neurite. In all groups, the prestimulus FWHM was greatest for the 4 mM Ca^{2+} group compared with the low $[\text{Ca}^{2+}]$ and $[\text{Sr}^{2+}]$ groups, probably because the baseline level exocytosis was more active at high $[\text{Ca}^{2+}]$. In the WT neurons, at 2.5 s and 5 s, the FWHM of all three ion conditions showed significant expansion, and the FWHM of the low $[\text{Ca}^{2+}]$ and $[\text{Sr}^{2+}]$ groups rapidly climbed to approach the level of 4 mM $[\text{Ca}^{2+}]$ (Fig. 4*E* and *F*). These results show that the exocytosis area expanded remarkably in response to the $\text{Ca}^{2+}/\text{Sr}^{2+}$ influx, indicating that the SVs in the peripheral AZ were competent for exocytosis. However, in the Syt7 KO neurons, the FWHM of all three groups increased very slowly, indicating that the spatial characteristics of the exocytosis were unaffected by changes in ion identity or concentration; namely, that the SVs in the peripheral AZ were relatively reluctant to release. In addition, reexpression of Syt7^{FL} in the KO neurons could rescue the FWHM phenotype, whereas the introduction of Syt7^{IF4mut} had no such effect. Therefore, the Syt7 SNPs could not efficiently induce SV release in the peripheral AZ of hippocampal neurons.

Retargeting Syt7 to the Central AZ Triggered Glutamate Release but Could Not Activate GluN2B-NMDARs. To help elucidate the role of Syt7 in the activation of GluN2B-NMDARs, we redistributed Syt7 to the whole AZ by conjugating the C2 domains of Syt7 to a short N terminus 20-aa peptide of GAP43 (designated Syt7^{GAP43}), which has been previously used to anchor Syt1 in the AZ (35). Because the Syt7 antibody cannot effectively label Syt7^{GAP43}, we used HA-tagged Syt7^{GAP43} (Syt7^{GAP43}-HA) for STORM analysis and observed that it was extensively distributed across the AZ (Fig. 5*A* and *B*). We then carried out a patch clamp recording analysis in cultured hippocampal neurons. The results indicated that

in Syt7 KO neurons, reexpression of Syt7^{GAP43} significantly reduced the amplitude of single AP-evoked AMPAR-EPSCs but failed to rescue the accelerated amplitude depression of train EPSCs (Fig. 5*C–F*). The attenuation of SV release may have occurred because Syt7^{GAP43} could compete with Syt1 for SVs and SNAREs.

We next analyzed the train-evoked NMDAR-EPSCs in 0.2 mM $[\text{Ca}^{2+}]$ (Fig. 5*G*). The KO neurons expressing Syt7^{GAP43} showed a reduced total charge transfer compared with the WT neurons (Fig. 5*H*). Similar to our results in the slices, Ro25-6981 application induced a significantly reduced charge transfer in the cultured WT neurons, whereas the Syt7 KO neurons were unaffected. Moreover, the deficits in the efficacy of Ro25-6981 in the KO neurons were rescued by Syt7^{FL} but not by Syt7^{GAP43}. We also analyzed the delayed charge by evaluating the decay time constant and observed similar results (Fig. 5*H*). Therefore, the Syt7^{GAP43} distributed across the AZ was able to trigger glutamate release; however, this failed to activate the GluN2B-NMDARs.

Syt7 Deficit-Induced GluN2B Dysfunction in BD Patient iPSC-Derived Hippocampal Neurons. In the final step, we aimed to ascertain whether deficits in the Syt7-GluN2B pathway existed in the iPSC-derived neurons of BD patients. To this end, we investigated the iPSC-derived hippocampal DG-like neurons of six patients with sporadic type I BD (BD-I) and four healthy control subjects (36). STORM analysis revealed that in the healthy control neurons, Syt7 was largely localized ~100 nm away from the central AZ; moreover, the BD-I patient iPSC-derived neurons showed significantly reduced Syt7 expression compared with the control group (Fig. 6*A* and *B*), which is consistent with our previous report (4). Furthermore, in the healthy control neurons, GluN2B was ~100 nm away from the central PSD, and in the diseased neurons, the distribution of GluN2B was unchanged, but its expression was increased (Fig. 6*C*). Immunoblot analysis confirmed the enhanced expression of GluN2A/2B in the patient neurons (Fig. 6*D*).

We then performed patch clamp recordings to analyze the train-evoked NMDAR-EPSCs in 0.2 mM Ca^{2+} . The assayed neurons showed strong expression of Prox1, a DG-specific marker, and normal AP firing (Fig. 6*E*). Although the patient neurons generally showed a trend toward enhancement of the total charge transfer compared with controls, the overall charge was only slightly increased (Fig. 6*F* and *G*). Furthermore, in the healthy control neurons, the Ro25-6981 treatment induced an attenuation in NMDAR-EPSCs, whereas the diseased neurons were only slightly affected (Fig. 6*H*). In addition, we carried out a rescue experiment in the neurons of three patients through lentiviral overexpression of Syt7^{FL} and found that the defective Ro25-6981 response could be restored by the expression of Syt7^{FL}. Taken together, our results indicate that the BD patient iPSC-derived hippocampal neurons showed Syt7 deficit-induced GluN2B dysfunction, which could be restored by the exogenous introduction of Syt7.

Discussion

Syt7 Triggers SV Release in the Peripheral AZ. AP-evoked SV release involves a bulk Ca^{2+} -triggered fast synchronous release and a residual Ca^{2+} -triggered asynchronous release. Residual Ca^{2+} also plays important roles in short-term presynaptic plasticity. Previous studies have suggested that during repetitive electrical stimulation, the synchronous and asynchronous phases of AP-evoked SV release are negatively correlated, probably due to a potential competition for the vesicles within the RRP (37, 38). However, although Syt7 has also been suggested to be a high-affinity Ca^{2+} sensor for asynchronous release, loss of Syt7 would lead to an impairment in fast synchronous release during repetitive stimulation, which seems contradictory (10, 11). Thus, it has been challenging to reconcile the functions of Syt7. In the present study, our SIM and STORM analyses revealed that Syt7 triggered SV release specifically in the peripheral AZ and

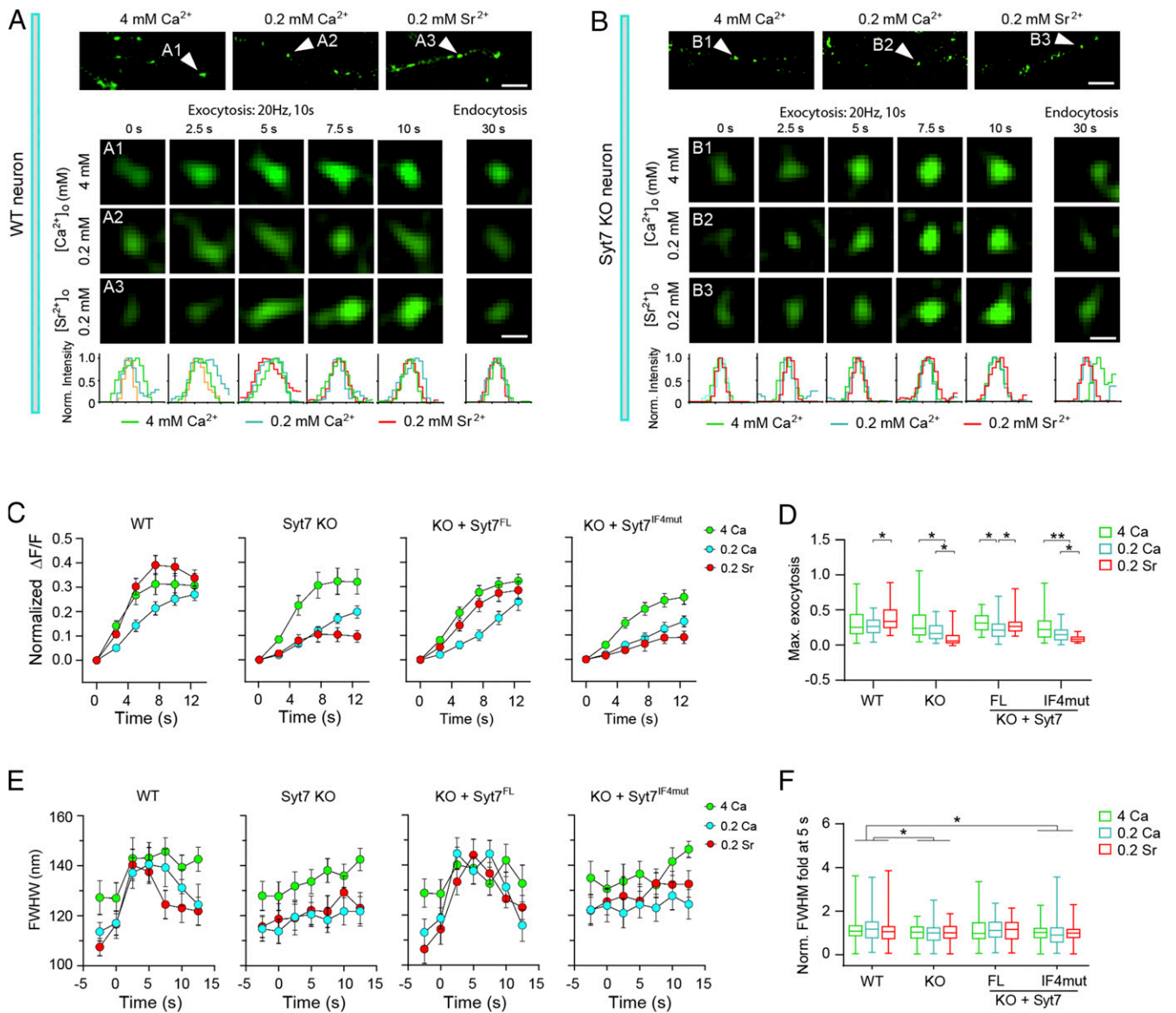


Fig. 4. Monitoring Syt7-triggered SV exocytosis in the peripheral active zone using SIM imaging. (A and B) Sample SIM images of sypHy-indicated SV exocytosis in WT (A) and Syt7 KO (B) hippocampal neurons. (Top) Sample images showing sypHy-indicated presynaptic boutons. (Scale bar: 1 μm .) (Middle) Time-lapse changes in the fluorescence of boutons indicated by the arrowheads in the Top images. (Scale bar: 200 nm.) (Bottom) Fluorescence intensity projected onto the x-axis. (C) Quantitative analysis of sypHy-measured overall SV exocytosis. WT, $n = 98$ to 104; Syt7 KO, $n = 94$ to 101; KO + Syt7^{FL}, $n = 76$ to 95; KO + Syt7^{IF4mut}, $n = 64$ to 88. (D) The ratio of maximal SV exocytosis. (E) The FWHM of SypHy puncta during the train stimulation. (F) Changes in the FWHM at 5 s relative to the 0 s values. * $P < 0.05$; ** $P < 0.001$, Student's t test. Error bars represent SEM.

this was unlikely to be in physical contact with the majority of SVs in the RRP. The SVs within the small Syt7-dominated pool efficiently responded to residual Ca²⁺ and thus could indiscriminately participate in low [Ca²⁺]-triggered SV release, including both asynchronous release and short-term plasticity. The locally functioning feature of Syt7 could explain why its absence causes parallel but not opposing changes in these two types of SV release.

It was recently suggested that in postsynaptic dendritic spines, Syt7 has a redundant Ca²⁺ sensor role together with Syt1 to mediate AMPAR trafficking during LTP, but that Syt7 deficiency alone does not have this effect (13). In the present study, our immunoblot and patch clamp recording analyses revealed that the expression and function of Syt1 and AMPARs were unchanged in the Syt7 KO neurons (Fig. 2 and *SI Appendix, Fig.*

S2). Furthermore, our results of the STORM analysis indicated that in the Syt7 KO neurons and the patient iPSC-derived neurons, the distribution of GluN2B was unchanged compared with that in controls. The experimental approaches that we used could exclude disturbance from postsynaptic effects. For instance, in the electrophysiological experiments, the 1-s duration of the train stimulation was very short, so that the recorded NMDAR-EPSCs were unlikely to be affected by changes in NMDAR trafficking. Moreover, in the SIM experiments, although the stimulation was elongated to 10 s, the fluorescence changes of sypHy exclusively represented bona fide presynaptic vesicle fusion events and thus would not be affected by any postsynaptic effect either. Therefore, the GluN2B hypoactivity that we observed was most likely a presynaptic, not a postsynaptic, consequence of Syt7 deficiency.

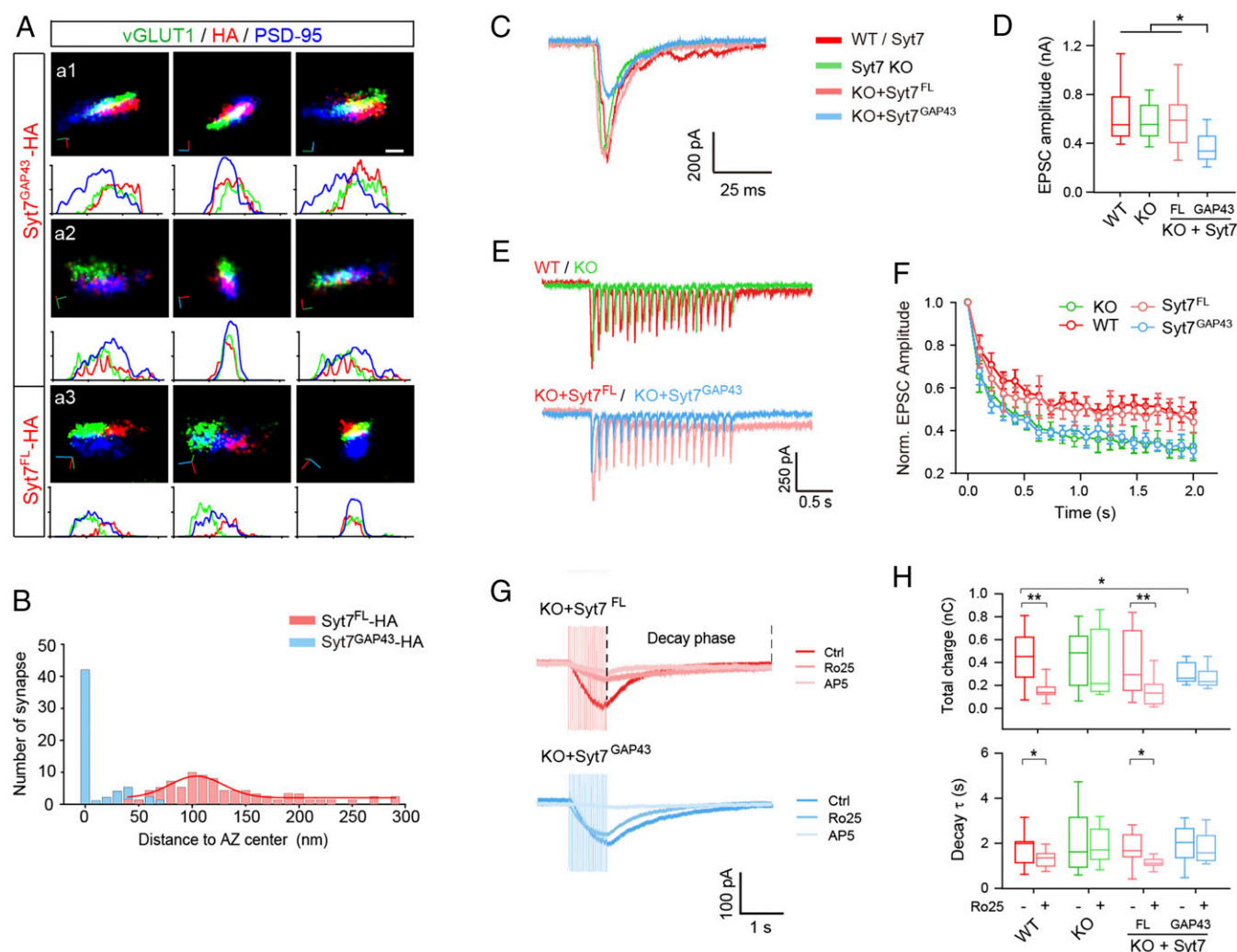


Fig. 5. Retargeting Syt7 to the central AZ triggers glutamate release but could not activate GluN2B-NMDARs. (A) Representative STORM images showing two sample synapses (a1 and a2) and a sample synapse expressing Syt7^{FL}-HA (a3). (Scale bar: 100 nm.) (B) Histogram showing the distances of Syt7^{GAP43}-HA ($n = 58$) and Syt7^{FL}-HA ($n = 81$) to the center of the AZ. The red curve is the fitted Gaussian curve for Syt7^{GAP43}-HA. (C and D) Representative traces (C) and mean amplitude (D) of evoked EPSCs recorded in WT ($n = 18$), Syt7 KO ($n = 18$), and KO neurons expressing Syt7^{FL} ($n = 15$) or Syt7^{GAP43} ($n = 21$). (E and F) Representative traces (E) and normalized amplitude (F) of 2-s, 10-Hz train stimulation evoked EPSCs. $n = 11$ to 17. (G) Sample traces of NMDAR-EPSCs triggered by 0.2 mM Ca²⁺ train stimulation. (H) Total charge transfer (Upper) and decay time constant (Lower) of NMDAR-EPSCs. $n = 14$ for all groups. * $P < 0.05$; ** $P < 0.001$, Student's t test. Error bars indicate SEM.

GluN2B Hypoactivity Contributes to the Induction of Mania-Like Behavioral Abnormalities in Mice. It has been widely accepted that antagonizing NMDARs can generate antidepressant effects; this consequence is mostly based on the blockade of the GluN2B subunit (16–18, 39). A number of studies have suggested that GluN2B-containing NMDARs have only a small, if any, role in AP-triggered neurotransmission, leading to the hypothesis that GluN2B is distributed extrasynaptically. However, some studies have produced evidence that GluN2B can respond to AP-evoked glutamate release. In the present study, our superresolution imaging and electrophysiological analyses revealed that GluN2B was present in the peripheral region of the PSD and was largely activated by AP-triggered asynchronous glutamate release. As this type of release in general accounts for a wide range (i.e., 0 to 30%) of the total AP-evoked SV exocytosis (32, 40), depending on experimental conditions including neuronal subtypes, it might lead to different observations regarding the activity of GluN2B in response to AP firing. In the present study, we applied 0.2 mM Ca²⁺ to recapitulate the action of residual Ca²⁺ influx in driving asynchronous SV release while synchronous release was largely

avoided. Using this approach, we provided solid evidence that GluN2B-NMDARs could be significantly activated by Syt7-triggered asynchronous glutamate release. Our findings should help resolve the discrepancies in the distribution and function of GluN2B.

In the present study, we observed that the Syt7 KO mice showed moderate responses to the application of GluN2B-NMDAR antagonists. Ketamine is a NMDAR antagonist that has been approved for the clinical treatment of major depressive disorder and bipolar depression. Interestingly, during the treatment of bipolar depression, ketamine rarely caused mania or hypomania, although it always induced mania in healthy people and nonpsychiatric patients (19–24), as did other drugs that act through attenuating glutamatergic transmission, such as lamotrigine and riluzole (25, 26). In contrast, tricyclic antidepressants and modulators of serotonin/dopamine/acetylcholine signaling systems often show severe mood-switching issues (25). In the present study, using MK-801 and Ro25-6981 as examples, our results demonstrate a mechanism by which the drugs targeting glutamatergic transmission can avoid overcorrection effects

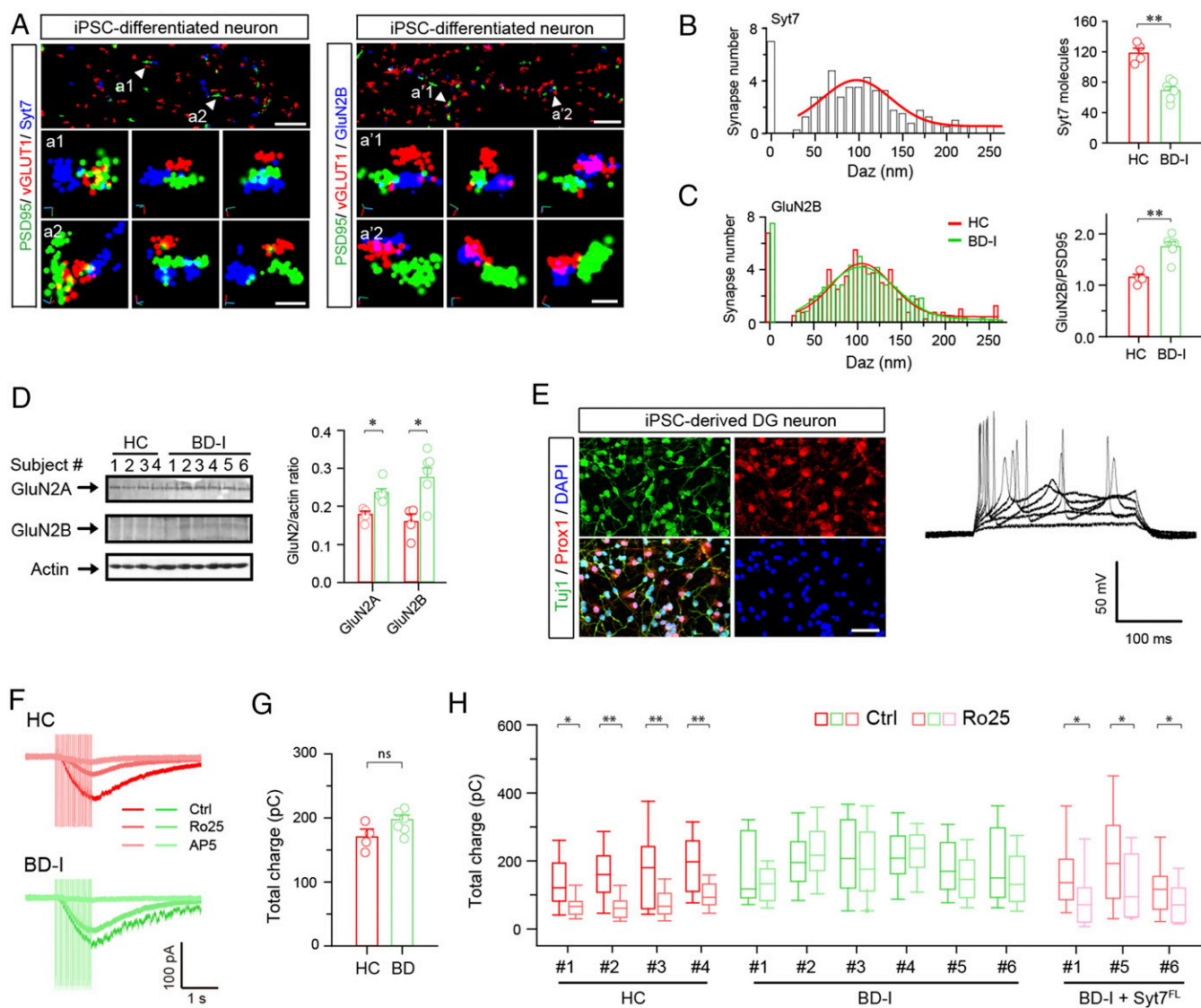


Fig. 6. Syt7 and GluN2B deficits in patient iPSC-derived hippocampal DG-like neurons. (A) Sample STORM images showing localization of Syt7 (Left) and GluN2B (Right) in the synapses of healthy control (HC) iPSC-derived neurons. Arrowheads denote sample synapses. (B) Histograms showing localization of Syt7 in the synapses of HC neurons (Left) and Syt7 expression in HC and patient iPSC-derived neurons (Right). HC, $n = 204$ synapses/4 subjects; BD-I, $n = 306/6$. (C) Localization (Left) and quantitative analysis (Right) of GluN2B in the synapses detected by STORM. (D) Immunoblots (Left) and quantitative analysis (Right) of GluN2A/2B in the patient iPSC-derived DG-like neurons. HC, $n = 4$ lines; BD, $n = 3$ for LR and $n = 3$ for NR. (E) Characterization of patient iPSC-derived DG-like neurons. (Left) Sample immunostaining images showing Prox1⁺ expression in the iPSC-derived neurons. (Scale bar: 50 μ m.) (Right) Sample traces showing evoked APs in Prox1⁺ neurons. (F) Sample traces of 1-s, 20-Hz train-triggered NMDAR-EPSCs recorded in patient iPSC-derived neurons in 0.2 mM Ca²⁺. (G) Comparison of NMDAR-EPSC charge transfer between the neurons of HC and patients. HC, $n = 4$ lines; BD-I, $n = 6$ lines. (H) Total charge transfer of NMDAR-EPSCs in HC neurons, BD-I neurons, and BD-I neurons overexpressing Syt7. HC, $n = 13$ to 51 for each cell line; BD-I, $n = 17$ to 43 for each cell line; BD-I + Syt7^{FL}, $n = 11$ to 26 for each cell line. * $P < 0.05$; ** $P < 0.001$, Student's t test. Error bars represent SEM.

when used for the treatment of depressive-like behavioral abnormalities. In addition to the Student's t test, we further analyzed the data using two-way ANOVA to verify our conclusions (SI Appendix, Fig. S3). Therefore, glutamatergic transmission could be an appropriate target for the development of new drugs for treating bipolar depression.

Initiating Mechanistic Research of Syt7 from the Hippocampus. In this present study, we have identified a mechanism used by Syt7 in the hippocampus to induce mania-like behaviors. The hippocampus has been shown to play important roles in the control of emotions, and acute manipulation of hippocampal neuronal activity can generate changes in mood-related behaviors (41–43). The hippocampus has also been suggested to be involved in a

variety of neuropsychiatric and neurodegenerative disorders, such as schizophrenia, BD, and Alzheimer's disease (44, 45). For instance, in BD patients, the number of neurons in the hippocampus is obviously reduced (45, 46). The hippocampal DG-like neurons derived from BD patients showed a phenotype of hyperactive AP firing. This neuronal hyperexcitability was accompanied by reduced Syt7 expression. Consistent with these findings, inactivation of Syt7 solely in the mouse hippocampus was sufficient to induce neuropsychiatric-like behavioral abnormalities. Thus, hippocampal neurons are likely to exhibit phenotypes of BD. Therefore, we chose to interrogate the mechanism of mania-like behaviors in the hippocampus. However, Syt7 is highly expressed in a variety of brain regions and likely has effects on the release of multiple types of neurotransmitters. Moreover, Syt7 is also expressed in

some peripheral organs, such as pancreatic islets. Consequently, the actual mechanism of how Syt7 can induce the swings of mania- and depression-like behaviors is much more complicated than what we have observed in the hippocampus and likely involves multiple brain regions and possibly peripheral organs.

Materials and Methods

Human Participants. A total of 1,456 inpatients (708 males and 748 females) age 19 to 65 y (mean age, 33 ± 12.19 y) with BD-I (average age at onset, 27.69 ± 10.47 y) according to the International Classification of Diseases, Tenth Revision criteria were recruited from the First Bethune Hospital of Jilin University between 2014 and 2017. Criteria for excluding patients from our analyses included preexisting history of brain organic diseases or other intercurrent clinical body diseases, head trauma, psychosis, hypophrenia, seizure, severe medical conditions, and alcoholism or drug abuse and pregnant or breastfeeding women. Meanwhile, 1,202 healthy subjects (544 males and 662 females) were also recruited from local communities as age-, sex-, and education level-matched controls. Criteria for excluding patients within the control group included a history of major psychiatric or neurologic disorders, severe head or birth trauma, febrile convulsion, adopted or single parent in childhood, and family history of inherited psychiatric or neurologic disorders. All of the participants were of Chinese Han origin. Written informed consent was obtained from all patients and controls. This study was approved by the Ethics Committees of the Chinese Academy of Medical Sciences and Peking Union Medical College.

- M. Ruzickova, C. Slaney, J. Garnham, M. Alda, Clinical features of bipolar disorder with and without comorbid diabetes mellitus. *Can. J. Psychiatry* **48**, 458–461 (2003).
- T. Hajek, R. McIntyre, M. Alda, Bipolar disorders, type 2 diabetes mellitus, and the brain. *Curr. Opin. Psychiatry* **29**, 1–6 (2016).
- A. Wysokiński, D. Strzelecki, I. Kloszewska, Levels of triglycerides, cholesterol, LDL, HDL and glucose in patients with schizophrenia, unipolar depression and bipolar disorder. *Diabetes Metab. Syndr.* **9**, 168–176 (2015).
- W. Shen *et al.*, Synaptotagmin-7 is a key factor for bipolar-like behavioral abnormalities in mice. *Proc. Natl. Acad. Sci. U.S.A.* **117**, 4392–4399 (2020).
- A. Bhalla, W. C. Tucker, E. R. Chapman, Synaptotagmin isoforms couple distinct ranges of Ca^{2+} , Ba^{2+} , and Sr^{2+} concentration to SNARE-mediated membrane fusion. *Mol. Biol. Cell* **16**, 4755–4764 (2005).
- B. Wu *et al.*, Synaptotagmin-7 phosphorylation mediates GLP-1-dependent potentiation of insulin secretion from β -cells. *Proc. Natl. Acad. Sci. U.S.A.* **112**, 9996–10001 (2015).
- N. Gustavsson *et al.*, Impaired insulin secretion and glucose intolerance in synaptotagmin-7 null mutant mice. *Proc. Natl. Acad. Sci. U.S.A.* **105**, 3992–3997 (2008).
- H. Wen *et al.*, Distinct roles for two synaptotagmin isoforms in synchronous and asynchronous transmitter release at zebrafish neuromuscular junction. *Proc. Natl. Acad. Sci. U.S.A.* **107**, 13906–13911 (2010).
- T. Bacaj *et al.*, Synaptotagmin-1 and synaptotagmin-7 trigger synchronous and asynchronous phases of neurotransmitter release. *Neuron* **80**, 947–959 (2013).
- H. Liu *et al.*, Synaptotagmin 7 functions as a Ca^{2+} sensor for synaptic vesicle replenishment. *eLife* **3**, e01524 (2014).
- S. L. Jackman, J. Turecek, J. E. Belinsky, W. G. Regehr, The calcium sensor synaptotagmin 7 is required for synaptic facilitation. *Nature* **529**, 88–91 (2016).
- Y. C. Li, N. L. Chanaday, W. Xu, E. T. Kavalali, Synaptotagmin-1- and Synaptotagmin-7-dependent fusion mechanisms target synaptic vesicles to kinetically distinct endocytic pathways. *Neuron* **93**, 616–631.e3 (2017).
- D. Wu *et al.*, Postsynaptic synaptotagmins mediate AMPA receptor exocytosis during LTP. *Nature* **544**, 316–321 (2017).
- J. León-Caballero *et al.*, Bipolar disorder and antibodies against the N-methyl-D-aspartate receptor: A gate to the involvement of autoimmunity in the pathophysiology of bipolar illness. *Neurosci. Biobehav. Rev.* **55**, 403–412 (2015).
- N. Li *et al.*, mTOR-dependent synapse formation underlies the rapid antidepressant effects of NMDA antagonists. *Science* **329**, 959–964 (2010).
- A. E. Autry *et al.*, NMDA receptor blockade at rest triggers rapid behavioural antidepressant responses. *Nature* **475**, 91–95 (2011).
- O. H. Miller *et al.*, GluN2B-containing NMDA receptors regulate depression-like behavior and are critical for the rapid antidepressant actions of ketamine. *eLife* **3**, e03581 (2014).
- C. Kisilewicz, P. Svenningsson, E. Delpire, A. Holmes, Genetic, pharmacological and lesion analyses reveal a selective role for corticohippocampal GLUN2B in a novel repeated swim stress paradigm. *Neuroscience* **193**, 259–268 (2011).
- A. K. Ricke, R. J. Snook, A. Anand, Induction of prolonged mania during ketamine therapy for reflex sympathetic dystrophy. *Biol. Psychiatry* **70**, e13–e14 (2011).
- A. McGirr *et al.*, A systematic review and meta-analysis of randomized, double-blind, placebo-controlled trials of ketamine in the rapid treatment of major depressive episodes. *Psychol. Med.* **45**, 693–704 (2015).
- N. Diazgranados *et al.*, A randomized add-on trial of an N-methyl-D-aspartate antagonist in treatment-resistant bipolar depression. *Arch. Gen. Psychiatry* **67**, 793–802 (2010).
- N. Lally *et al.*, Anti-anhedonic effect of ketamine and its neural correlates in treatment-resistant bipolar depression. *Transl. Psychiatry* **4**, e469 (2014).
- A. Z. Zarate Jr *et al.*, Replication of ketamine's antidepressant efficacy in bipolar depression: A randomized controlled add-on trial. *Biol. Psychiatry* **71**, 939–946 (2012).
- A. K. Parsaik, B. Singh, D. Khosh-Chashm, S. S. Mascarenhas, Efficacy of ketamine in bipolar depression: Systematic review and meta-analysis. *J. Psychiatr. Pract.* **21**, 427–435 (2015). Retraction in: *J. Psychiatr. Pract.* **24**, 307 (2018).
- A. Muneer, Mixed states in bipolar disorder: Etiology, pathogenesis and treatment. *Chonnam Med. J.* **53**, 1–13 (2017).
- R. S. McIntyre, D. S. Cha, R. D. Kim, R. B. Mansur, A review of FDA-approved treatment options in bipolar depression. *CNS Spectr.* **18** (suppl. 1), 4–20, quiz 21 (2013).
- S. Maeng *et al.*, Cellular mechanisms underlying the antidepressant effects of ketamine: Role of alpha-amino-3-hydroxy-5-methylisoxazole-4-propionic acid receptors. *Biol. Psychiatry* **63**, 349–352 (2008).
- C. Kisilewicz *et al.*, NMDA receptor subunits and associated signaling molecules mediating antidepressant-related effects of NMDA-GluN2B antagonism. *Behav. Brain Res.* **287**, 89–95 (2015).
- C. Ribault, K. Sekimoto, A. Triller, From the stochasticity of molecular processes to the variability of synaptic transmission. *Nat. Rev. Neurosci.* **12**, 375–387 (2011).
- I. Pérez-Otaño, M. D. Ehlers, Homeostatic plasticity and NMDA receptor trafficking. *Trends Neurosci.* **28**, 229–238 (2005).
- G. G. Turrigiano, The self-tuning neuron: Synaptic scaling of excitatory synapses. *Cell* **135**, 422–435 (2008).
- J. Yao, J. D. Gaffaney, S. E. Kwon, E. R. Chapman, Doc2 is a Ca^{2+} sensor required for asynchronous neurotransmitter release. *Cell* **147**, 666–677 (2011).
- G. Miesenböck, D. A. De Angelis, J. E. Rothman, Visualizing secretion and synaptic transmission with pH-sensitive green fluorescent proteins. *Nature* **394**, 192–195 (1998).
- J. Turecek, W. G. Regehr, Synaptotagmin 7 mediates both facilitation and asynchronous release at granule cell synapses. *J. Neurosci.* **38**, 3240–3251 (2018).
- J. Yao, S. E. Kwon, J. D. Gaffaney, F. M. Dunning, E. R. Chapman, Uncoupling the roles of synaptotagmin I during endo- and exocytosis of synaptic vesicles. *Nat. Neurosci.* **15**, 243–249 (2011).
- J. Mertens *et al.*, Pharmacogenomics of Bipolar Disorder Study, Differential responses to lithium in hyperexcitable neurons from patients with bipolar disorder. *Nature* **527**, 95–99 (2015). Correction in: *Nature* **530**, 242 (2016).
- D. J. Hagler Jr, Y. Goda, Properties of synchronous and asynchronous release during pulse train depression in cultured hippocampal neurons. *J. Neurophysiol.* **85**, 2324–2334 (2001).
- Y. Otsu *et al.*, Competition between phasic and asynchronous release for recovered synaptic vesicles at developing hippocampal autaptic synapses. *J. Neurosci.* **24**, 420–433 (2004).
- D. Atasoy *et al.*, Spontaneous and evoked glutamate release activates two populations of NMDA receptors with limited overlap. *J. Neurosci.* **28**, 10151–10166 (2008).
- H. Liu, C. Dean, C. P. Arthur, M. Dong, E. R. Chapman, Autapses and networks of hippocampal neurons exhibit distinct synaptic transmission phenotypes in the absence of synaptotagmin I. *J. Neurosci.* **29**, 7395–7403 (2009).
- M. A. Kheirbek *et al.*, Differential control of learning and anxiety along the dorsoventral axis of the dentate gyrus. *Neuron* **77**, 955–968 (2013).
- S. Ramirez *et al.*, Activating positive memory engrams suppresses depression-like behaviour. *Nature* **522**, 335–339 (2015).
- Y. Zheng *et al.*, CRISPR interference-based specific and efficient gene inactivation in the brain. *Nat. Neurosci.* **21**, 447–454 (2018).
- S. F. Sonnenschein, F. V. Gomes, A. A. Grace, Dysregulation of midbrain dopamine system and the pathophysiology of schizophrenia. *Front. Psychiatry* **11**, 613 (2020).
- R. F. Deicken, M. P. Pegues, S. Anzalone, R. Feiwell, B. Soher, Lower concentration of hippocampal N-acetylaspartate in familial bipolar I disorder. *Am. J. Psychiatry* **160**, 873–882 (2003).
- A. Bertolino *et al.*, Neuronal pathology in the hippocampal area of patients with bipolar disorder: A study with proton magnetic resonance spectroscopic imaging. *Biol. Psychiatry* **53**, 906–913 (2003).